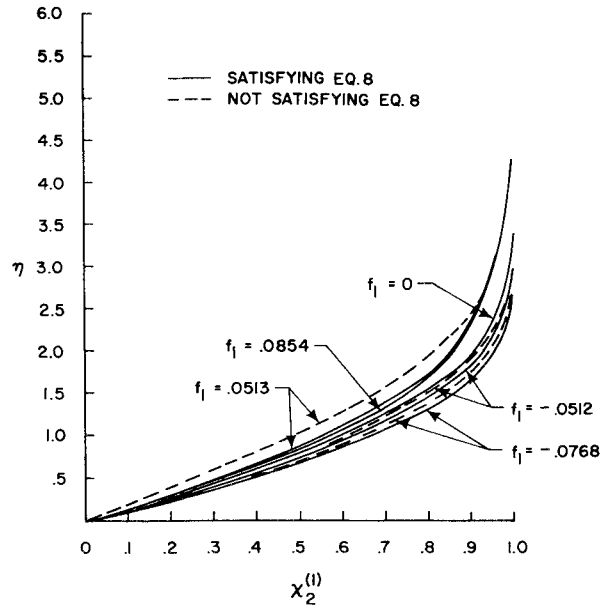

Fig. 2 Spanwise boundary-layer profiles $\chi_2^{(1)}$ as functions of η.

$$P_1(f_1) = \alpha^2 + (2f_1/f_{1s})(f_{1s} - \alpha^2/2), \quad -f_{1s} \leqq f_1 \leqq f_{1s} \tag{9}$$

For surfaces satisfying Eq. (8), we have $P_1(f_1) = P_2(f_1)$ where P_1 is defined in Eq. (9). For surfaces which do not satisfy Eq. (8), the $P_2(f_1)$ distribution is chosen as

$$P_2(f_1) = P_1(f_1) + C\alpha^2 f_1/f_{1s}[1 - (f_1/f_{1s})]^{1/2} \tag{10}$$

Good comparison with the results of Refs. 2 and 5 was obtained by taking $C = -8$ and $C = 4$ for the ranges $0 \leqq f_1 \leqq f_{1s}$ and $-f_{1s} \leqq f_1 \leqq 0$ respectively.

Equations (3–5) with $P_{1,2}(f_1)$ replacing $U^2\theta_x^2/\nu\tilde{\phi}_1$ and $U^2\theta_x^2 \cos\beta/\nu\tilde{X}$ have been solved by an implicit finite-difference method for values of f_1 in the range $-f_{1s} \leqq f_1 \leqq f_{1s}$, where $f_{1s} = 0.0854$. In this range the tabulated values of $\partial\phi^{(1)}/\partial\eta$ are available in Ref. 4. The boundary conditions for Eqs. (3–5) are

$$\eta = 0: \ \chi_1^{(1)} = \chi_2^{(1)} = \chi_3^{(1)} = 0$$

$$\eta \to \infty: \ \chi_1^{(1)}, \chi_2^{(1)}, \text{ and } \chi_3^{(1)} \to 1$$

Initial conditions were prescribed at $f_1 = f_{1s}$ where $\chi_1^{(1)}$, $\chi_2^{(1)}$, and $\chi_3^{(1)}$ satisfy the ordinary differential equations whose solutions are known.

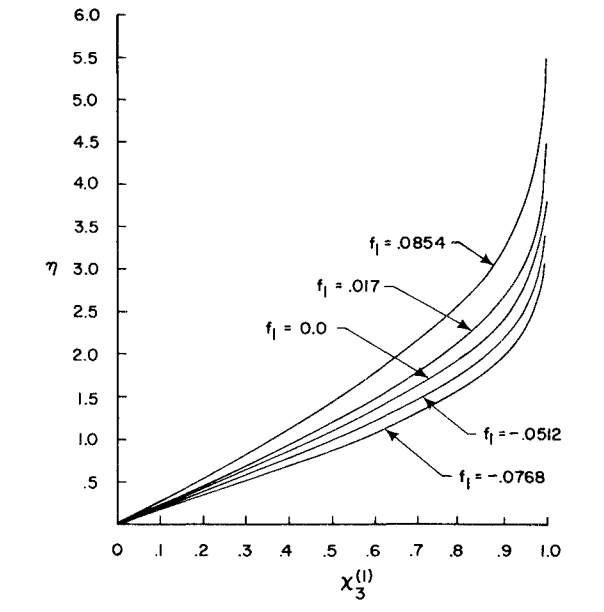

Fig. 3 Spanwise boundary-layer profiles $\chi_3^{(1)}$ as functions of η.

Figures 1–3 represent the values of $\chi_1^{(1)}$, $\chi_2^{(1)}$, and $\chi_3^{(1)}$ for various values of f_1. Tabulated values of the chordwise velocity distributions are avilable in Ref. 4. In any practical problem one has only to prescribe the nondimensional external velocity $U(x)$ and then the values of f_1 are obtained by the recurrence relation [Eqs. (21) and (22) of Ref. 1]

$$U^b Z^*(x_n) = U^b(x_{n-1}) Z^*(x_{n-1}) + (a + \varepsilon_{n-1}) \int_{x_{n-1}}^{x_n} U^{b-1}(x)\,dx \tag{11}$$

where $Z^* = \theta_x^2/\nu$ and $a = 0.4408$, $b = 5.714$. The function $\varepsilon_{n-1} = \varepsilon_{n-1}(f_1)$ is plotted in Ref. 1.

Results and Discussion

The universal solutions of the rotating blade boundary-layer equations are presented for blades of sufficiently long spans. These solutions can be used for a quick and direct assessment of the velocity distribution on a given blade. The steps are as follows: 1) For a given external velocity distribution first nondimensionalize and normalize as given in Eq. (2b). 2) Prepare the table for $Z^*(x)$; Eq. (11). 3) Check to see whether Eq. (8) is satisfied. For this case, data of Fig. 1, Fig. 2 (continuous lines), and Fig. 3 have to be used. 4) If Eq. (8) is not satisfied, then Fig. 1, Fig. 2 (broken lines), and Fig. 3 have to be used.

References

[1] Warsi, Z. U. A., "Further Theoretical Investigation of the Laminar Boundary Layer over Rotating Blades and Yawed Infinite Wings," *AIAA Journal*, Vol. 7, No. 4, April 1969, pp. 687–693.

[2] Fogarty, L. E., "The Laminar Boundary Layer on a Rotating Blade," *Journal of the Aeronautical Sciences*, Vol. 18, No. 4, April 1951, pp. 247–252.

[3] Rott, N. and Smith, W. E., "Some Examples of Laminar Boundary Layer Flow on Rotating Blades," *Journal of the Aeronautical Sciences*, Vol. 23, No. 11, Nov. 1956, pp. 991–996.

[4] Loitsianskii, L. G., "The Universal Equations and Parametric Approximations in the Theory of the Laminar Boundary Layers," *PMM*, Vol. 29, No. 1, 1965, pp. 74–92.

[5] Graham, M., "Calculation of Laminar Boundary Layer Flow on Rotating Blades," Ph.D. thesis, Sept. 1954, Cornell University, Ithaca, N.Y.

Postbuckling Behavior of Clamped Skew Plates

M. S. S. PRABHU* AND S. DURVASULA†
Indian Institute of Science, Bangalore, India

POSTBUCKLING behavior of skew plates has not received adequate attention. Recently, Ref. 1 dealt with the postbuckling behavior of orthotropic skew plates. However, the results presented therein exhibit some incorrect trends. In a study of the postbuckling behavior of isotropic clamped skew plates, we were interested in examining the use of two alternative schemes in solving the problem. The first one is the Galerkin method with the Newton-Raphson (N-R) procedure, and the second is the Perturbation method. Some of the results of this investigation are reported briefly in this Note.

Received January 29, 1974; revision received May 7, 1974.
Index category: Structural Stability Analysis.

* Formerly Research Student, Department of Aeronautical Engineering; presently Engineer, Indian Scientific Satellite Project, Bangalore.
† Associate Professor, Department of Aeronautical Engineering.

A sketch of the skew plate with oblique coordinate system and oblique stress system is shown in Fig. 1 as an inset. The postbuckling behavior of skew plates under the action of in-plane forces is governed by von Kármán equations which, in terms of nondimensional coordinates $\xi(=x/a)$ and $\eta(=y/b)$ and nondimensional parameters $\bar{F}(=F/D)$ and $\bar{W}[=W(1-\nu^2)^{1/2}/h]$ can be written as

$$\nabla^4 \bar{F} = -\lambda^2 \cos^2\psi \diamond^4(\bar{W}, \bar{W})$$
$$\nabla^4 \bar{W} = \lambda^2 \cos^2\psi \diamond^4(\bar{W}, \bar{F}) \tag{1}$$

where ∇^4 is biharmonic operator,

$$\diamond^4 \left(= \frac{\partial^2}{\partial\xi^2}\frac{\partial^2}{\partial\eta^2} - 2\frac{\partial^2}{\partial\xi\,\partial\eta}\frac{\partial^2}{\partial\xi\,\partial\eta} + \frac{\partial^2}{\partial\eta^2}\frac{\partial^2}{\partial\xi^2} \right)$$

is the die-operator, and $\lambda(=a/b)$ is the aspect ratio. The oblique components of stress are related to the stress function as

$$\sigma_x = \sec\psi F_{,\eta\eta}/b^2h; \quad \sigma_y = \sec\psi F_{,\xi\xi}/a^2h;$$
$$\sigma_{xy} = -\sec\psi F_{,\xi\eta}/hab \tag{2}$$

The boundary conditions of a clamped plate under the action of σ_x alone and with traction free unloaded edges can be written as

$$F_{,\eta\eta} = -\sigma_x hb^2 \cos\psi, \quad F_{,\xi\eta} = 0, \quad \text{on} \quad \xi = -1 \quad \text{and} \quad 1$$
$$F_{,\xi\xi} = F_{,\xi\eta} = 0, \quad \text{on} \quad \eta = -1 \quad \text{and} \quad 1$$
$$W = W_{,\xi} = 0, \quad \text{on} \quad \xi = -1 \quad \text{and} \quad 1 \tag{3}$$
$$W = W_{,\eta} = 0, \quad \text{on} \quad \eta = -1 \quad \text{and} \quad 1$$

Thus, the problem reduces to obtaining a solution to two coupled nonlinear partial differential equations, Eq. (1), together with boundary conditions, Eq. (3). We employ two procedures to obtain approximate solution to these equations: first, using the Galerkin method to reduce the governing equations to a set of nonlinear algebraic equations and then using the Newton-Raphson technique to obtain a solution to this set; and second, using the perturbation method to reduce the nonlinear differential equations to a set of linear differential equations and then solving this set of linear differential equations by the Galerkin method.

Procedure 1: Galerkin Method and Newton-Raphson Technique

The stress function F and deflection $\bar{W}$ are expanded in a series of functions as

$$\bar{W} = \sum_{m=1}^{M}\sum_{n=1}^{N} w_{mn}\bar{X}_m(\xi)\bar{Y}_n(\eta)$$
$$F = \sum_{m=1}^{P}\sum_{n=1}^{Q} f_{mn}X_m(\xi)Y_n(\eta) - (\sigma_x hb^2\cos\psi)\eta^2/2 \tag{4}$$

Suitable polynomials are chosen for the functions such that each combination $\bar{X}_m\bar{Y}_n$ and X_mY_n satisfies the relevant boundary conditions of Eq. (3). Substituting the expressions for $\bar{W}$ and F in Eq. (1) and applying the Galerkin method, we obtain a set of nonlinear algebraic equations in unknowns f_{mn}'s and w_{mn}'s. To facilitate discussion, let x_i denote the $(M+1)$ unknown coefficients f_{mn}'s and w_{mn}'s and in-plane loading parameter $\bar{R}_x(=-\sigma_x hb^2/D)$. It is often convenient to include $\bar{R}_x$ also as dependent variable thus making $(M+1)$ coefficients and then treating any one of the coefficients as an independent variable. This results in faster convergence and also avoids the difficulty of the Jacobian matrix becoming singular and the consequent failure of the N-R method[2] when $\bar{R}_x$ is near its critical value. The resulting set of equations which may be denoted by Y, for simplicity, can be represented as

$$Y = P_j(x_i) + Q_j(x_{M+1}) = 0, \quad i,j = 1,2\ldots M \tag{5}$$

The solution after n iterations can be written as

$$\{x_i\}_{n+1} = \{x_i\}_n - [\partial P_j/\partial x_i]_n\{Y\}_n \tag{6}$$

The successive approximations are compared and if the difference is within a preassigned value, the iterations are halted and $\{x_i\}_{n+1}$ is taken as the solution to the set of nonlinear equations.

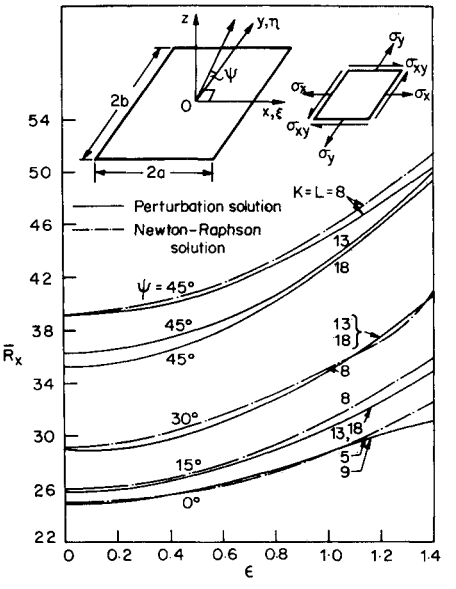

Fig. 1 Variation of in-plane load parameter $\bar{R}_x$ with central deflection parameter ε.

Procedure 2: Perturbation Method

The stress function $\bar{F}$ and deflection $\bar{W}$ are expanded in a power series of ascending powers of a suitable perturbation parameter ε as

$$\bar{W}(\xi,\eta) = \sum_{n=1,3}\varepsilon^n W_n(\xi,\eta); \quad \bar{F}(\xi,\eta) = \sum_{n=0,2}\varepsilon^n F_n(\xi,\eta) \tag{7}$$

The choice of a perturbation parameter, in general, is arbitrary. However, in this study, the central deflection parameter $\bar{W}(0,0)$, is chosen for ε. Substituting the above series for W and $\bar{F}$ in the differential equations, (1), and boundary conditions, Eq. (3), and equating terms of different powers of ε, we obtain approximations of different orders. The linear partial differential equations correspond to the different orders of approximation of the perturbation method which would be the plane stress problem, the eigenvalue problem, and the nonlinear problem, respectively. They are then solved by using the Galerkin method with polynomials for stress functions F_n's, and deflection functions W_n's.

Results and Discussion

Figure 1 shows the relationship between $\bar{R}_x$ and the central deflection parameter ε for different skew angles. Results obtained by both methods are given for comparison. The number of terms in $\bar{W}$ and $\bar{F}$ is denoted by K and L, respectively. For the same number of terms considered, there is close agreement between the results by the two methods. However, considering the effort involved in terms of computer time, it is felt that the perturbation method is definitely preferable since it requires, for a given geometry, only one solution for the complete spectrum of load whereas in the N-R method, a solution is to be obtained for each value of $\bar{R}_x$ (or any other independent variable).

The effect of nonlinearity is examined in Table 1. The critical values of Ref. 1 along with accurate estimates for eigenvalues obtained by using beam characteristic functions[3] also are given. It can be seen that while the buckling coefficients of the present study are quite accurate, the expression of Ref. 1 based on a one-term approximation for deflection leads to a crude estimate of the buckling coefficient even for small skew angles. For higher skew angles, the expression of Ref. 1 leads to completely unreliable results; for example, for $\psi = 60°$ and $\lambda = 1$, it yields $\bar{R}_x = 117$, while the estimate of Ref. 3 is as low as 19.7 which is a well converged estimate. It is observed that

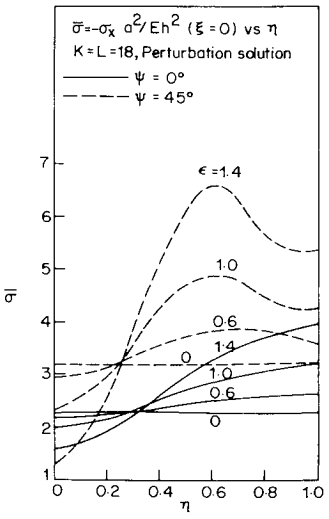

Fig. 2 Membrane stress distribution along $\xi = 0$ for different values of ε.

Table 1 Effect of nonlinearity

		$\bar{R}_x = \bar{R}_{x\text{crit}}(1 + K_2\varepsilon^2 + K_4\varepsilon^4 + \cdots)$				
		$\bar{R}_{x\text{crit}}$				
ψ	Number of terms in $\bar{W}$ and F $K = L$	Present note	Ref. 1	Ref. 3	K_2	K_4
0°	9	25.0	26.4	24.9	0.19	−0.03
15°	18	25.8	39.0	25.8	0.20	−0.01
30°	18	28.9	55.8	28.9	0.21	−0.0002
45°	18	35.3	93.0	35.1	0.21	0

the nonlinearity represented mainly by K_2, coefficient of ε^2, is of a hardening type and tends to remain nearly constant with increasing skew angle.

This also is reflected in the curves of Fig. 1 as they tend to be roughly parallel. In fact, if $\bar{R}_x/\bar{R}_{x\text{crit}}$ is plotted against the deflection parameter ε, the curves for the various skew angles of Fig. 1 of the present Note would be confined to a narrow band unlike the curves of Ref. 1 which indicate that the effect of nonlinearity decreases considerably with increase in skew angle. It may be mentioned here that the near constancy of the magnitude of nonlinearity with skew angle also is depicted in the load vs end shortening plots for different ψ's which are not presented here for the sake of brevity.

Figure 2 shows the variation of membrane stress σ_x along the center line of the plate for different values of the deflection parameter ε for two different skew angles. The magnitude of stress increases with deflection and also with skew angle. For $\psi = 0°$, the location of maximum stress remains on the edge as deflection increases. For $\psi = 45°$, however, the location of maximum stress shifts inwards with increasing deflection. Further, a detailed study of stress distribution for different skew angles shows that this shift increases with skew angle.

References

[1] Pandalai, K. A. V. and Satyamoorthy, M., "Postbuckling Behavior of Orthotropic Skew Plates," *AIAA Journal*, Vol. 11, No. 5, May 1973, pp. 731–733.

[2] Leicester, R. H., "Finite Deformations of Shallow Shells," *Proceedings of ASCE, Journal of Engineering Mechanics Division*, Vol. 94, No. EM6, Dec. 1968, pp. 1409–1423.

[3] Mahabaliraja and Durvasula, S., "Design Data on Buckling of Clamped Skew Plates (Oblique Components), Part—I: Individual Loading," Rept. AE 296 S, May 1971, Dept. of Aeronautical Engineering, Indian Institute of Science, Bangalore, India.

Transition Prediction Technique

J. A. Benek* and M. D. High†
ARO, Inc., Arnold Air Force Station, Tenn.

Introduction

One of the first boundary-layer transition correlations based upon a theoretical foundation was given by Liepman[1] who hypothesized that laminar breakdown occurred when the ratio of inertial to viscous stresses obtained a critical value. He then used linear stability theory to relate this ratio to flow variables. There have been many subsequent and moderately successful correlation schemes based upon either the Liepmann hypothesis or linear stability theory.[2] The most important in the context of this paper is that of Van Driest and Blumer.[3]

There have also been numerous experimental investigations of the transition process.[4–9] A common feature of these investigations is that the test facility influences the results by introducing either vorticity or acoustic disturbances into the free-stream flow. The manner in which the magnitude of these disturbances varies depends upon the flow regime and test facility. However, the common trend is that as the disturbance magnitude increases, the transition Reynolds number decreases.

Analysis

Liepmann's hypothesis can be written as a critical Reynolds number

$$R_{\text{crit}} = (\rho\overline{u_i u_j})/(\mu\, du/dy)$$

where $\rho\overline{u_i u_j}$ is the inertial or Reynolds stress and $\mu\, du/dy$ is the viscous stress. The critical value, R_{crit}, can be expected to occur somewhere in the interior of the boundary layer, say at $y = y_c$. This expression can be put in a more suitable form for calculation by eliminating $\overline{u_i u_j}$ by using the Prandlt mixing length hypothesis, and then by using Pohlhausen's velocity profile to evaluate the velocity gradient. The critical Reynolds number then has the form

$$R_{\text{crit}} = Re_l^2/\delta[F'(\eta_c) + \Lambda G'(\eta_c)] \tag{1}$$

where F and G are polynomials in η, $\eta = y/\delta$, δ is the boundary-layer thickness, Re is the unit Reynolds number, l is the mixing length, and Λ for compressible flow is

$$\Lambda = (\rho_\infty/\rho_w)(\delta^2)/(v_\infty \rho_\infty u_\infty)(\partial P/\partial x)$$

where ρ_∞/ρ_w is the ratio of freestream to wall density, v_∞ is the kinematic viscosity, and $\partial P/\partial x$ is the pressure gradient.

The effects of the disturbances can be entered through the pressure gradient, if the pressure is assumed to be linearly composed of a mean pressure, $\bar{p}$, and two fluctuating pressures, $\tilde{p}_v$ and $\tilde{p}_a$ where $\tilde{p}_v$ is due to vorticity, and $\tilde{p}_a$ is due to acoustic disturbances. Further, since the vorticity fluctuations are primarily velocity fluctuations, we can use Taylor's[10] relation $\tilde{p}_v \simeq \bar{\rho}(\tilde{u})^2$ where $\tilde{u}$ is the rms velocity fluctuation due to vorticity variations. Thus

$$\Lambda = -\delta^2(\rho_\infty/\rho_w)/v_\infty \rho_\infty u_\infty)[\chi\, \partial\bar{P}/\partial x + F\rho\tilde{u}^2/\lambda_v + Z\tilde{P}_a/\lambda_a]$$

where χ, λ_v, λ_a are appropriate scale lengths. The coefficient $F = (1+40M_f)^{1/2}$ (Ref. 11) is a compressibility correction to $\tilde{p}_v$, where $M_f = \tilde{u}/u_\infty$. For small fluctuations (i.e., $\tilde{u}$ small), $F \simeq 1.0$.

Received February 7, 1974; revision received May 28, 1974. The research reported herein was conducted by the Arnold Engineering Development Center, Air Force Systems Command. Research results were obtained by personnel of ARO, Inc., Contract Operator at AEDC. Further reproduction is authorized to satisfy needs of the U.S. Government.

Index category: Boundary-Layer Stability and Transition.

* Research Engineer, 16T/16S Projects Branch, Propulsion Wind Tunnel Facility. Member AIAA.

† Supervisor, 16T/16S Projects Branch, Propulsion Wind Tunnel Facility. Associate Fellow AIAA.